

# Dual-Guest Functionalised Zeolitic Imidazolate Framework-8 for 3D Printing White Light-Emitting Composites

*Abhijeet K. Chaudhari and Jin-Chong Tan\**

Multifunctional Materials & Composites (MMC) Laboratory, Department of Engineering Science, University of Oxford, Parks Road, Oxford, OX1 3PJ, United Kingdom.

*\*E-mail: jin-chong.tan@eng.ox.ac.uk*

## Abstract

Metal-organic frameworks (MOFs) stand as a promising chemically active host scaffold for the encapsulation of functional guests, because they could enhance luminescent properties by molecular separation of fluorophores in the nanoscale pores of the MOF crystals. Herein, we show simultaneous nanoconfinement of two fluorophores *viz.* (A) Fluorescein and (B) Rhodamine B in the sodalite cages of ZIF-8, constructed under ambient conditions through a simple one-pot reaction. We report a novel dual-guest@MOF system, termed: A+B@ZIF-8, which overcomes the intrinsic problem of aggregation caused quenching in the solid-state to gain bright yellow emission under UV irradiation. Subsequently, we combine this yellow emitter with a blue-emitting photopolymer resin, to yield a 3D printable luminescent composite material. We design a number of 3D printable composite objects for converting UV into warm white light emission, achieving a high quantum yield of ~44% in the solid-state 3D printed form. This research instigates the bespoke application of a vast range of 3D printable Guest@MOF designer composites targeting energy-saving lighting devices, smart sensors and future optoelectronics.

## 1. Introduction

World's 20% of energy is consumed by lighting on planet earth.<sup>[1-2]</sup> Consequently, substantial research in material science is focussed on the search for alternative solutions to yield more efficient solid-state lighting with enhanced quantum yield and emission lifetime.<sup>[2-3]</sup> In the pursuit of new materials, current research has concentrated on white light generation using luminescent organic molecules, polymers with red-green-blue (RGB) emitting side chains, three-layer RGB molecular system, hybrid perovskites, supramolecular polymers and lanthanide-based phosphor-converted white light-emitting diodes.<sup>[4-8]</sup> In the case of phosphor-converted white light-emitting diodes (LEDs), phosphors are composed of rare-earth elements that not only are of a limited supply, but also pose health hazards<sup>[9]</sup> and serious environmental impact.<sup>[10]</sup> In the light of this, there is an urgent need to develop and discover alternative materials to enable next-generation solid-state lighting applications.

The self-assembly of metal-organic frameworks (MOFs) or porous coordination polymers (PCPs) in an orderly fashion to form periodic framework structures offers several advantages.<sup>[11-13]</sup> More recently, researchers are exploring the use of periodic chemically-active molecular spaces found in the nanoscale pores of MOFs/PCPs (acting as a 'host' framework) to confine a range of functional 'guest' species or molecular complexes. The guest confinement approach yields a guest-host system termed 'Guest@MOF',<sup>[14]</sup> that can be useful as an electrical conductor,<sup>[15-16]</sup> light-emitting material,<sup>[17-19]</sup> selective gas/analyte sorbent, drug carrier, and chemical sensors.<sup>[20-21]</sup> For example, we have been working on a number of Guest@MOF systems to develop tuneable luminescent materials for photonics-based sensing applications.<sup>[22-24]</sup> In our studies, we found that the high concentration reaction (HCR) protocol is advantageous for: (i) rapid one-pot synthesis of nano-MOFs (e.g. nanosheets and nanostructures), (ii) *in situ* encapsulation of bulky guest molecules or nanoconfinement of metal complexes,

and (iii) high yield of end products under ambient conditions.<sup>[22]</sup> These characteristics are the main requirements for constructing a functional material *via* facile guest confinement, with easy processability and future industrial-scale synthesis.

There is an increasing number of studies on Guest@MOF research reporting the encapsulation of a wide range of functional guests, such as rare-earth metals, organic dyes, carbon dots, quantum dots, and metal complexes to achieve tuneable luminescent properties and white light generation.<sup>[17-19, 25-32]</sup> Indeed, the majority of current efforts are much dependent on the use of non-economical and non-environmentally friendly rare-earth metals, see the statistics in Figure S1 of the Supporting Information (SI). Additionally, recent examples of synthetic method adopted for constructing tuneable luminescent systems require multistep core-shell processing to yield multivariate guest encapsulation,<sup>[33]</sup> which may be challenging to translate from lab to practical applications.

Herein we demonstrate the use of the HCR approach to accomplish the *in situ* multi-guest encapsulation of two fluorescent dye species (rare-earth free guests), being nanoconfined within the sodalite cage of the ZIF-8 framework *via* a one-pot reaction under ambient conditions. First, we present the facile synthesis and detailed characterisation of the previously unreported ‘A+B@ZIF-8’ compound (where, A: Fluorescein and B: Rhodamine B), which has a nanodisc morphology and emits yellow fluorescence (see Figure 1). Subsequently, we show how this new yellow-light emitter can be easily combined with a blue light-emitting photopolymer to form a composite that can be readily printed using a commercial 3D stereolithography machine. Finally, we demonstrate warm white light-emitting 3D printed objects and performed detailed characterisation of their photophysical properties central to the engineering of functional applications.

## 2. Results and Discussion

### 2.1 Rapid synthesis of dual-guest@MOF system

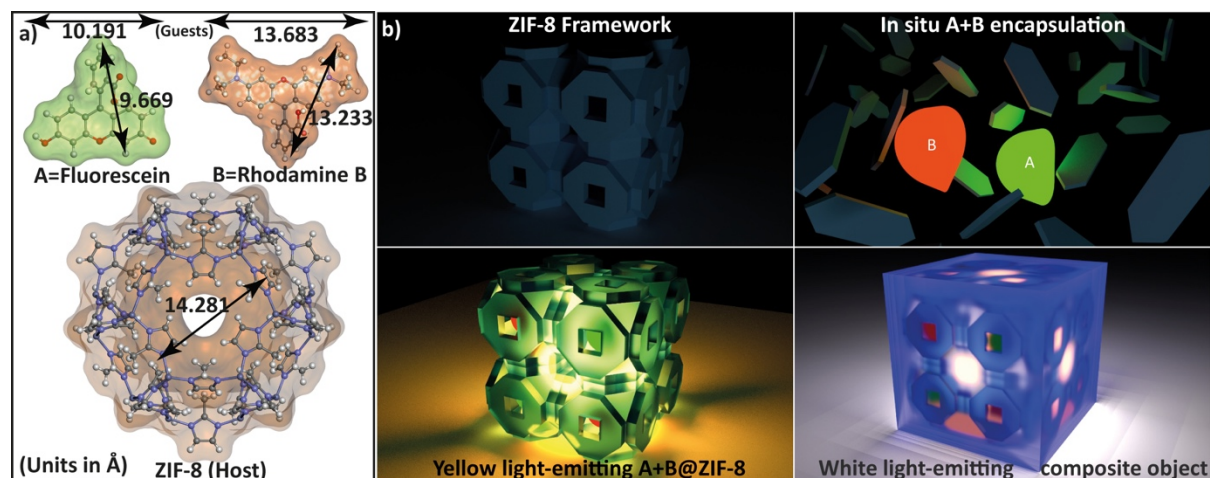


**Figure 1.** (a) Structural dimensions of the two fluorescent guest species A and B, and the host framework of ZIF-8 used in the current study. (b) Schematic representation of the concept adopted to fabricate A+B@ZIF-8 through *in situ* dual-guest encapsulation strategy, resulting in yellow-light emission in the solid state. Its subsequent use for fabricating a white-light emitting 3D object, which is a composite material of A+B@ZIF-8 combined with a blue light-emitting clear photopolymer resin.

On the one hand, we chose ZIF-8 as the host material because of its relatively large pore size within its sodalite cage (despite having small pore windows, see Figure 1a) together with its ease of synthesis. On the other hand, we chose Fluorescein (hereby denoted as ‘A’) and Rhodamine B (denoted as ‘B’) as the two fluorescent guest species for having strong green- and red-light emissions, respectively. Both the guests are ideal based on their molecular sizes and their ability to be constrained with the help of flexible/rotating groups like diethylamine ( $\text{NEt}_2$ ) and phenyl-COOH in a nanoconfined environment (Figure 1a). Because of spatial constraints, it is possible for one dye species (A or B) to occupy a single pore cavity. The two different dye species, however, may be occupying adjacent pores of the assembled framework of the A+B@ZIF-8 compound. From the combination of both the dye molecules in methanol, we

successfully achieved a deep-yellow colour emission by adjusting their volume ratios (Figure 2a inset). It was found that a combination of 25 mL 0.1 mM Fluorescein and 1.25 mL 0.1 mM Rhodamine B solutions exhibit a strong yellow light-emission when irradiated under the 365-nm UV source. This homogenous solution of A+B was used directly for constructing the ‘Dual-Guest@MOF’ system. Here, the combination of solutions was the important precursor for attaining solid-state yellow light-emitting A+B@ZIF-8 powder. The next crucial step was HCR synthesis of ZIF-8 by combining 3 mmol (0.8923g) of  $\text{Zn}(\text{NO}_3)_2$  in 3 mL of methanol and 7.5 mmol (0.61575g) of deprotonated 2-methylimidazole (mIm) in 3 mL of methanol (mIm was deprotonated using 7.5 mmol in 1.04 mL of trimethylamine,  $\text{NEt}_3$ ) in the presence of the A+B methanolic solution.

By employing the HCR method,<sup>[22]</sup> we obtained a readily forming product as soon as the linker and metal ion solutions were mixed together in the presence of the A+B guest solution. The product formed was thoroughly washed using methanol (where both the A and B guests, as well as host reactants are highly soluble) to remove non-confined guest molecules, and the excess mIm and  $\text{Zn}^{2+}$  reactants. Further details of the synthesis are given in the SI (sections 2 and 3). Notably, the wet sample after washing and its dried powder have retained the yellow emission evidenced in the A+B solution combination (Figure 2a). Here, we note that the ZIF-8 host plays an important role by separating the single molecules from each other, thereby maintaining the solution-like optical properties that are generally quenched in the solid-state form of pure emitters (like A and B employed in the current study, see Figure S2). To confirm the successful framework formation and A+B guest confinement within it, material characterisation was performed. Powder X-ray diffraction (XRD) of the dry final product confirmed the formation of A+B@ZIF-8, without major changes to the original structure of ZIF-8, though some broadening of the Bragg peaks was noticed (Figure 2a). Morphological

characterisation of the compound using atomic force microscopy (AFM) revealed the nanodisc-like morphology with an aspect ratio ranging from 5:1 to 10:1, where each nanodisc exhibits a thickness of under  $\sim 20$  nm with a lateral dimension of over 100–200 nm (Figure 2b, and representative AFM images in Figures S5). The presence of nanostructures supports the broadening of XRD peaks observed in Figure 2a.

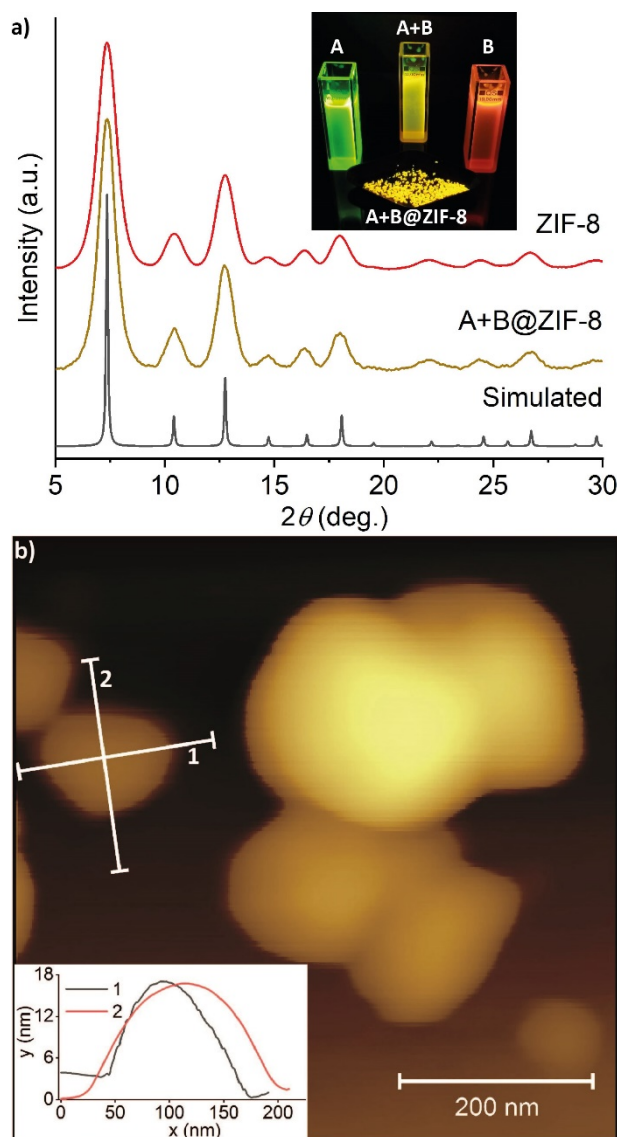


**Figure 2.** (a) X-ray diffraction of A+B@ZIF-8 powder confirming the crystal structure of ZIF-8 obtained by one-pot high-concentration reaction method. Inset shows the emissions observed under a 365 nm UV lamp: solid-state A+B@ZIF-8 powder and solution-state A+B combination, as compared with the pure solutions of (A) Fluorescein and (B) Rhodamine B in methanol. (b) Atomic force microscopy image of the A+B@ZIF-8 crystals exhibiting the nanodisc morphology, whose aspect ratio (length/height) is about 10:1 as shown in the inset.

## 2.2 3-D printing of light-emitting composite objects

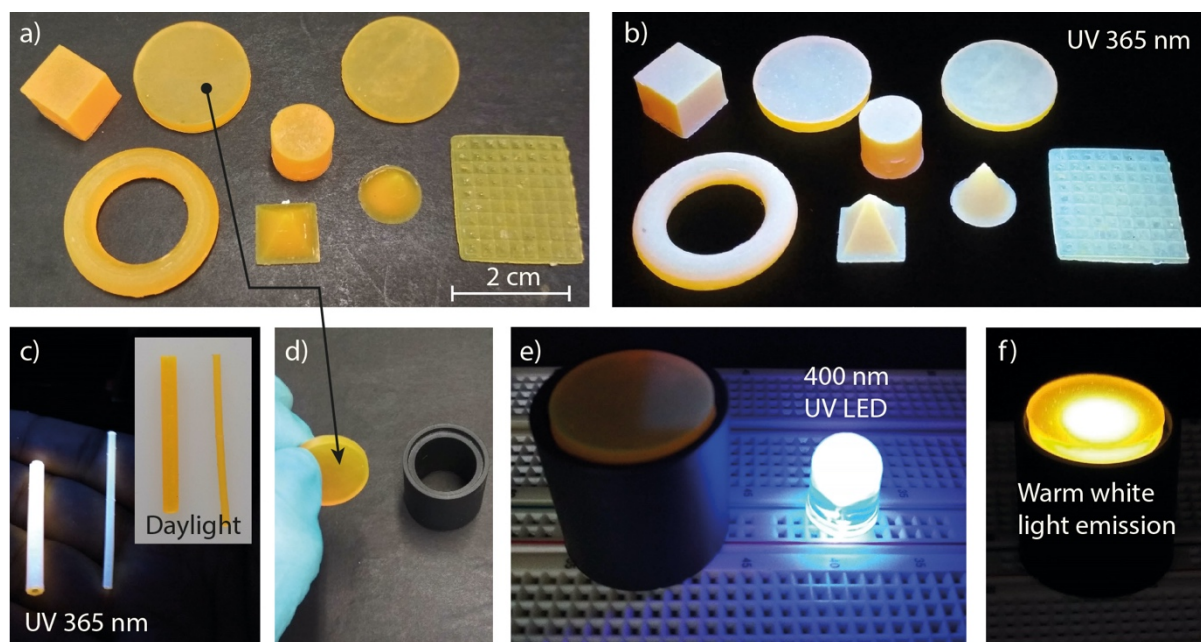


**Figure 3.** (a) Various shapes of 3D-printed objects constructed from the composite made of A+B@ZIF-8 powder dispersed in a clear photopolymer resin. (b-c) The 3D-printed composite produces white light emission under UV irradiation. (d) A 3-mm thick 3D printed disc-shaped pellet installed on a black cylindrical support (e) for converting 400 nm UV irradiation from an LED to generate (f) warm white-light emission.

Using the A+B@ZIF-8 powder, now we proceed with the creation of 3D-printed objects capable of generating a white light emission. A commercially available optically transparent photopolymer with blue emission under UV (‘clear resin’ by Formlabs, see SI section 4) was used for this purpose. We established that a combination of 10 g of yellow light-emitting A+B@ZIF-8 compound with 50 mL of blue light-emitting clear resin results in a stable white light-emitting composite after printing (Figure 3). The main strategy implemented here for obtaining a homogenous mixture of A+B@ZIF-8 and clear resin was the use of a wet sample of the former after thorough washing and centrifugation steps. The mixture was stirred together at room temperature for ~12 hours in the dark, to achieve homogeneity of the mixture while avoiding curing of resin by the

surrounding light (see Figure S3). This composite mixture stayed consistently homogenous after overnight mixing without visible agglomeration of solid particles. The mixture was directly used for printing a wide range of 3D objects shown in Figure 3a-c. In Figures 3d-f, we demonstrated a 3-mm thick 3D printed composite pellet for generating warm white light when exposed to a 400 nm UV LED. Colour chromaticity diagram in Figure 4 shows that the 3D printed composite (A+B@ZIF-8 in clear resin) could convert UV light, where the CIE coordinates were determined to change from ( $x$ ,  $y$ ) values of (0.1888, 0.1114) to (0.4117, 0.4790) hence shifting to a warm white light emission (defined in the range of about 3100-4500 K). Furthermore, we demonstrate that it is straightforward to tune the emission chromaticity to cover a broad range of colour temperatures, from cool to warm white light, by systematically changing the thickness of the 3D printed pellets. Figure 4b shows the evolution of the emission spectra as a function of pellet thickness. The systematic shift of CIE coordinates when varying the pellet thickness between 0.5 mm and 5.2 mm is demonstrated in Figure 4(c).



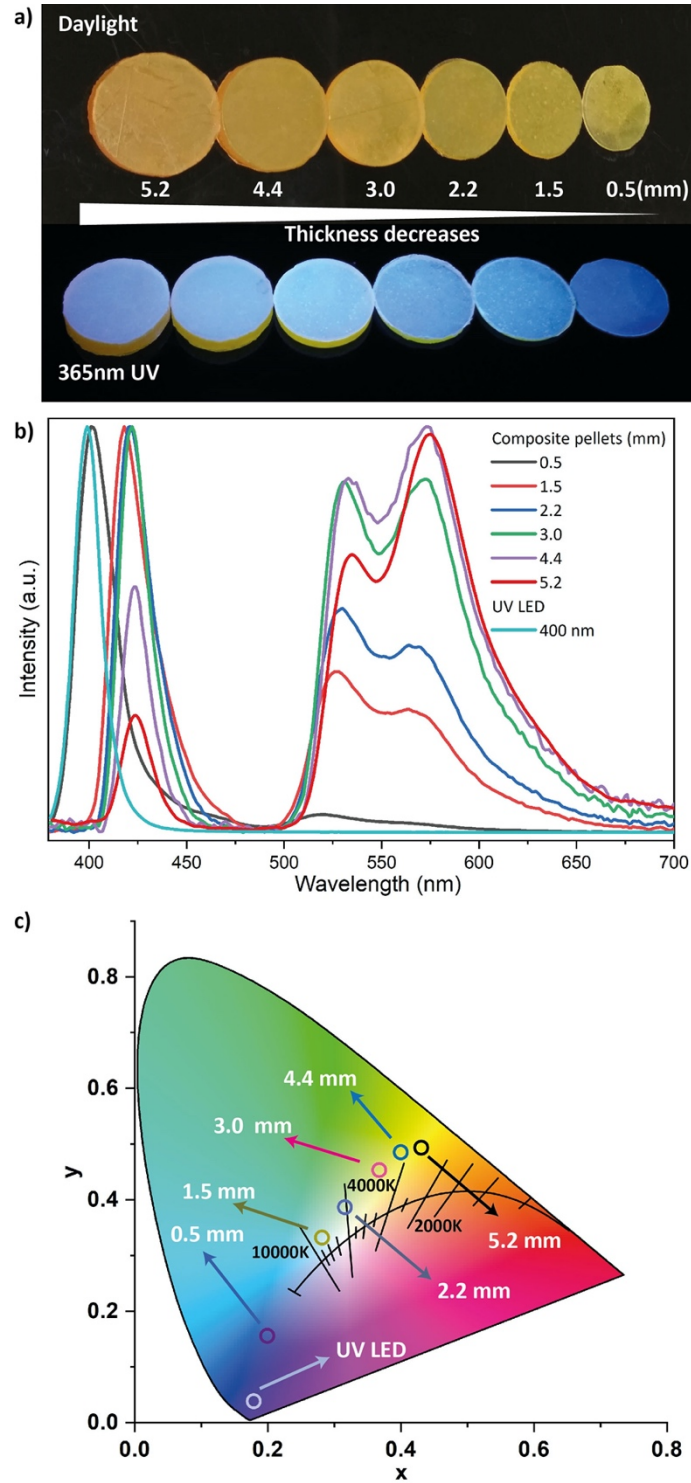


**Figure 4.** (a) Photograph taken under the 365-nm UV lamp, showing the emission of the 3D printed pellets of different thicknesses. (b) Tuneable pellet emission when being employed as the lid of a light conversion device (Figure 3f) and irradiated by a 400-nm UV LED. Note that the passage of the 400-nm UV source through the clear lid has been blocked by a thickness of between 0.5-1.5 mm. (c) CIE coordinates and colour

temperature showing the effects of pellet thickness, showing the ability for tuning the emission ranging from cool white light to warm white light.

### 2.3 Photophysical properties

We have investigated in detail the optical properties of the A+B@ZIF-8 compound and the resulting 3D-printed composites to understand the effects of confinement of fluorescent guests by the framework of ZIF-8, and when it is incorporated within the photopolymer resin. From the beginning we observed the bright emission arising from the solid-state powder of A+B@ZIF-8, which is a clear indication of single molecule separation of emissive guest species by the nanopores of ZIF-8. This observation was later confirmed by contrasting the solution-state and solid-state optical properties data shown in Figure 5.

Figure 5a shows the excitation spectra of the solutions and solids. Solution A (Fluorescein) has excitation maximum at 494 nm; at 496 nm in combination with solution B (Rhodamine B), and at 511 nm in A+B@ZIF-8 solid-state form as well as in the composite pellet form. Turning to solution B, it exhibits excitation maximum at 544 nm but retains this wavelength in combination with solution A; at 555 nm in A+B@ZIF-8 solid-state form, and at 554 nm in the composite pellet form.

Figure 5b compares the emission spectra of the solutions and solids. When excited, the emission maximum of solution A was observed at 515 nm; at 516 nm in combination with solution B, however it red shifted to 542 nm for A+B@ZIF-8 solid-state form and again blue shifted to 528 nm for the composite pellet form. In the case of solution B, emission maximum was observed at 570 nm, it maintained the same position in combination with solution A, but red shifted to 580 nm for A+B@ZIF-8 solid state form and again blue shifted to 572 nm for the composite pellet form. The emission spectra of the composite pellet are independent of the excitation wavelengths (Figure S5).

The modification to the photophysical properties of the fluorescent guest and the host framework discussed above reveal the effects of guest-host interaction. The major interacting groups at the ground state located around the environment of guest species are the -N-Zn-N- linkages and the H-C=C-H group of mIm, which can polarise A and B to alter their optical properties and resulting in the red shifted emission. For the 3D printed composite pellet, we reasoned that the observed blue shifted emission is due to the structural relaxation of A+B@ZIF-8 upon its dispersion in the resin photopolymer. Both guest species, A and B possess hydrogen bond-making and  $\pi$ - $\pi$  stacking phenyl-COOH group as well as the 'O' and 'N<sup>+</sup>' (for B) sites, which could easily interact with the surrounding framework environment. Moreover, the emission spectrum of the clear resin photopolymer exhibits emission maximum at 440 nm in the 3D-printed blank pellet versus 434 nm in the composite pellet. Interestingly, this means that the emission spectrum of resin has a strong overlap with the excitation spectra of A and B (Figure 5c), hence facilitating the excited-state energy transfer from the clear photopolymer resin to the confined guest emitters. For further comparison the diffuse reflectance spectra of the 3D printed pellet and its constituents in the solid state are shown in Figure S7, showing the overlapping absorption bands associated with host-guest interactions.

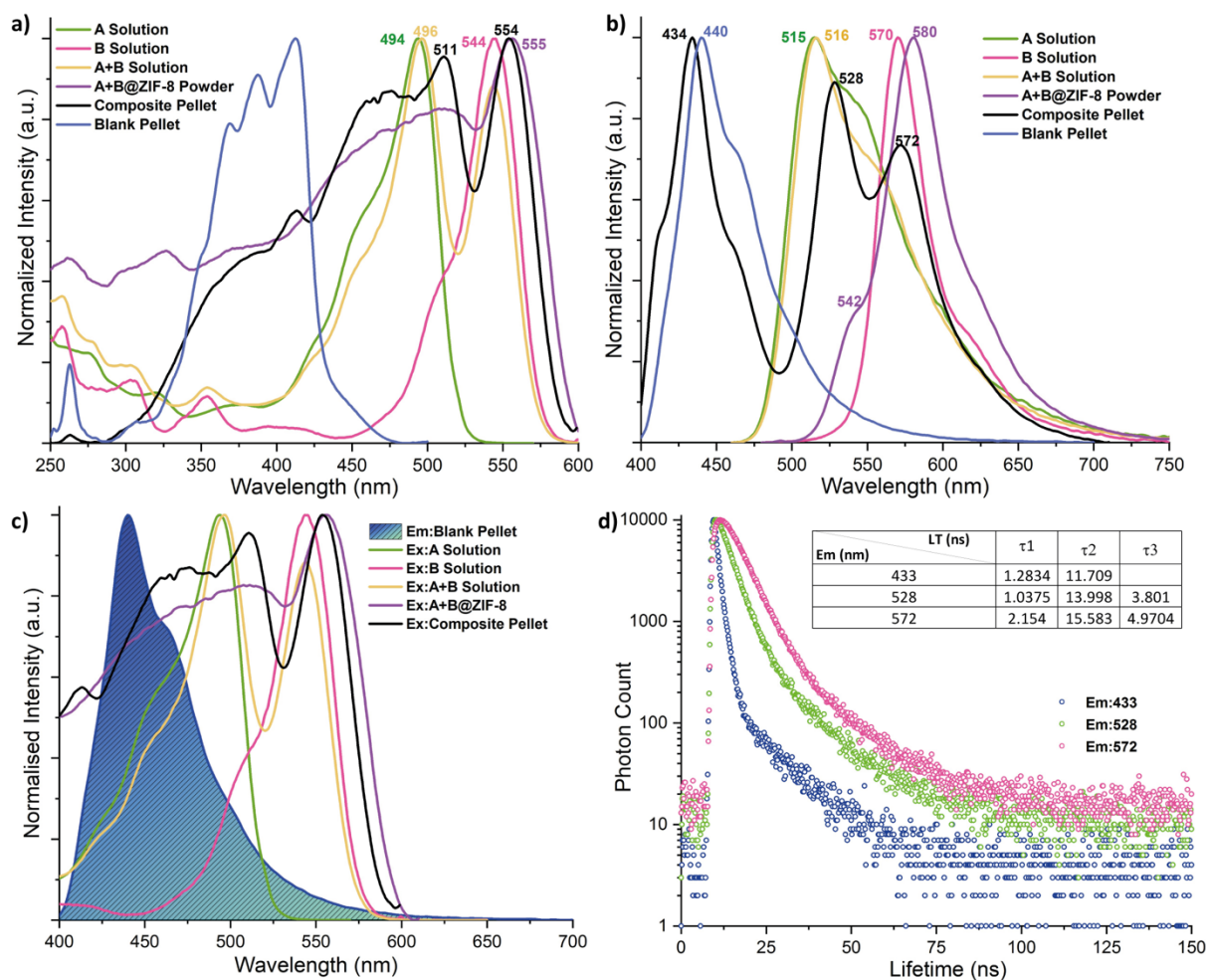


**Figure 5.** (a) Excitation and (b) emission spectra of the A and B guest species in solution form (isolated or combined), A+B@ZIF-8 in solid-state form (dual-guest@MOF powder), 3D printed blank pellet (photopolymer clear resin) and composite pellet (A+B@ZIF-8 combined with clear resin). (c) Emission spectrum of 3D printed blank pellet compared to the excitation spectra of other fluorescent species to identify overlap for energy transfer in excited state. (d) Fluorescence lifetime decay curves of the white light-emitting composite pellet measured at three different emission wavelengths, the table inset summarises the time constants ( $\tau$ ) in nanoseconds.

The energy transfer process was studied by fluorescence lifetime (FLT) measurements employing the time-correlated single photon counting (TCSPC) technique. Decrease in FLT with energy transfer from donor to acceptor is indicative of a non-radiative process as evidenced from FLT of the clear resin (blank pellet), which

fell from 15.40 ns to 13.99 ns (for emission at 528 nm), and to 11.70 ns (for emission at 433 nm). No major change in FLT of resin was observed for emission at 572 nm (see more details in Table S1). A short lifetime of ~2 ns corresponds to emission of the mIm linker of ZIF-8, the lifetime greater than 11 ns corresponds to the resin, while the lifetimes of 3.801 ns and 4.9704 ns can be ascribed to guest A and guest B, respectively. Detailed FLT data and curve fitting results are given in Figures S8-S17 in the SI. The quantum yield (QY) values of the A+B@ZIF-8 solid powder and the 3D-printed composite pellet are 47.3% and 43.6%, respectively (Table S2). In fact, their QY values are appreciably higher versus other solid-state Guest@MOF luminescent materials found in the literature, for example: QY = 30% for Zr-NDC MOF,<sup>[30]</sup> QY = 17.4% for ZJU-28,<sup>[28]</sup> and QY = 20.4% for iridium-complex@MOF.<sup>[17]</sup>

### 3. Conclusions

In summary, we show for the first time a Dual-Guest@MOF material which can be 3D printed to construct a warm white light-emitting device. In fact, the colour chromaticity of the device can be straightforwardly adjusted from a cool white light to a warm white light emission (CCT: 8300 K  $\rightarrow$  3700 K), simply by varying the thickness of the pellets. Our HCR synthetic protocol is versatile, as it enables simultaneous nanoscale confinement of multivariate fluorescent guest species within the MOF pores. Significantly, the separation of fluorescent dye molecules prevents the aggregation caused quenching phenomenon, therefore enabling bright light emission to be retained in the solid state. The facile one-pot synthetic strategy we demonstrated here is easy to implement and has a good yield in terms of materials production. It can be tailored for large-scale fabrication of fluorescent materials and adapted to confine multiple fluorescent dyes aimed at bespoke lighting applications. It is important to recognise that the direct addition of dye molecules into resin could not yield the same emission as

obtained from the dispersion of A+B@ZIF-8 in resin, because the dilution effect of unencapsulated dyes could alter the resultant emission spectra. Finally, we show the efficacy for combining fluorescent Guest@MOF compounds with a photopolymer resin to enable 3D printing of a wide range of geometries and designs, as such opening the door for the engineering of photonic sensors, optoelectronics, and future metamaterials. Our study therefore demonstrates the advantages of employing the Dual-Guest@MOF approach: on the one hand, to permit chromaticity tuning, and, on the other hand, for enhancing structural and photostability of functional devices *via* the manufacturing of 3D printed composite objects.

### **Acknowledgements**

We thank the ERC Consolidator Grant under the grant agreement 771575 (PROMOFS) for supporting the research. We are grateful to the Research Complex at Harwell (RCaH) for access to the materials characterization facilities.

### **Conflicts of interest**

There are no conflicts to declare.

## References

- [1] G. Zissis, in *Handbook of advanced lighting technology* (Eds.: R. Karlicek, C.-C. Sun, G. Zissis, R. Ma), Springer International Publishing, Cham, **2016**, pp. 1-13.
- [2] H. B. Wu, L. Ying, W. Yang, Y. Cao, *Chem. Soc. Rev.* **2009**, 38, 3391-3400.
- [3] M. D. Allendorf, C. A. Bauer, R. K. Bhakta, R. J. T. Houk, *Chem. Soc. Rev.* **2009**, 38, 1330-1352.
- [4] B. W. D'Andrade, S. R. Forrest, *Adv. Mater.* **2004**, 16, 1585-1595.
- [5] C. Fan, C. L. Yang, *Chem. Soc. Rev.* **2014**, 43, 6439-6469.
- [6] G. M. Farinola, R. Ragni, *Chem. Soc. Rev.* **2011**, 40, 3467-3482.
- [7] N. J. Findlay, J. Bruckbauer, A. R. Inigo, B. Breig, S. Arumugam, D. J. Wallis, R. W. Martin, P. J. Skabara, *Adv. Mater.* **2014**, 26, 7290-7294.
- [8] M. C. Gather, A. Kohnen, K. Meerholz, *Adv. Mater.* **2011**, 23, 233-248.
- [9] G. Pagano, M. Guida, F. Tommasi, R. Oral, *Ecotoxicol. Environ. Saf.* **2015**, 115, 40-48.
- [10] V. Balaram, *Geosci. Front.* **2019**, 10, 1285-1303.
- [11] B. F. Hoskins, R. Robson, *J. Am. Chem. Soc.* **1989**, 111, 5962-5964.
- [12] S. L. James, *Chem. Soc. Rev.* **2003**, 32, 276-288.
- [13] S. Kitagawa, R. Kitaura, S. Noro, *Angew. Chem. Int. Ed.* **2004**, 43, 2334-2375.
- [14] M. D. Allendorf, M. E. Foster, F. Leonard, V. Stavila, P. L. Feng, F. P. Doty, K. Leong, E. Y. Ma, S. R. Johnston, A. A. Talin, *J. Phys. Chem. Lett.* **2015**, 6, 1182-1195.
- [15] A. A. Talin, A. Centrone, A. C. Ford, M. E. Foster, V. Stavila, P. Haney, R. A. Kinney, V. Szalai, F. El Gabaly, H. P. Yoon, F. Leonard, M. D. Allendorf, *Science* **2014**, 343, 66-69.
- [16] I. Stassen, N. Burtch, A. Talin, P. Falcaro, M. Allendorf, R. Ameloot, *Chem. Soc. Rev.* **2017**, 46, 3185-3241.
- [17] C. Y. Sun, X. L. Wang, X. Zhang, C. Qin, P. Li, Z. M. Su, D. X. Zhu, G. G. Shan, K. Z. Shao, H. Wu, J. Li, *Nat. Commun.* **2013**, 4, 2717.
- [18] Y. Wen, T. Sheng, X. Zhu, C. Zhuo, S. Su, H. Li, S. Hu, Q. L. Zhu, X. Wu, *Adv. Mater.* **2017**, 29, 1700778.
- [19] Z. Wang, C. Y. Zhu, J. T. Mo, P. Y. Fu, Y. W. Zhao, S. Y. Yin, J. J. Jiang, M. Pan, C. Y. Su, *Angew. Chem. Int. Ed.* **2019**, 58, 9752-9757.

- [20] N. B. Shustova, A. F. Cozzolino, S. Reineke, M. Baldo, M. Dinca, *J. Am. Chem. Soc.* **2013**, *135*, 13326-13329.
- [21] M. R. Ryder, J. C. Tan, *Mater. Sci. Tech.* **2014**, *30*, 1598-1612.
- [22] A. K. Chaudhari, H. J. Kim, I. Han, J. C. Tan, *Adv. Mater.* **2017**, *29*, 1701463.
- [23] A. K. Chaudhari, M. R. Ryder, J. C. Tan, *Nanoscale* **2016**, *8*, 6851-6859.
- [24] A. K. Chaudhari, J. C. Tan, *Nanoscale* **2018**, *10*, 3953-3960.
- [25] A. W. Wang, Y. L. Hou, F. W. Kang, F. C. Lyu, Y. Xiong, W. C. Chen, C. S. Lee, Z. T. Xu, A. L. Rogach, J. Lu, Y. Y. Li, *J. Mater. Chem. B* **2019**, *7*, 2207-2211.
- [26] H. Cai, L. L. Xu, H. Y. Lai, J. Y. Liu, S. W. Ng, D. Li, *Chem. Commun.* **2017**, *53*, 7917-7920.
- [27] J. Heine, K. Muller-Buschbaum, *Chem. Soc. Rev.* **2013**, *42*, 9232-9242.
- [28] Y. Cui, T. Song, J. Yu, Y. Yang, Z. Wang, G. Qian, *Adv. Funct. Mater.* **2015**, *25*, 4796-4802.
- [29] J. Cornelio, T. Y. Zhou, A. Alkas, S. G. Telfer, *J. Am. Chem. Soc.* **2018**, *140*, 15470-15476.
- [30] M. Gutierrez, C. Martin, K. Kennes, J. Hofkens, M. Vander Auweraer, F. Sanchez, A. Douhal, *Adv. Opt. Mater.* **2018**, *6*, 1701060.
- [31] W. P. Lustig, J. Li, *Coord. Chem. Rev.* **2018**, *373*, 116-147.
- [32] Y. Tang, T. F. Xia, T. Song, Y. J. Cui, Y. Yang, G. D. Qian, *Adv. Opt. Mater.* **2018**, *6*, 1800968.
- [33] Y. F. Chen, B. Yu, Y. D. Cui, S. J. Xu, J. B. Gong, *Chem. Mater.* **2019**, *31*, 1289-1295.